Available online at www.sciencedirect.com
ScienceDirect
Polymer 47 (2006) 8548–8555
polymer
www.elsevier.com/locate/polymer

Partial delamination of the organo-montmorillonite with surfactant containing hydroxyl groups in maleated poly(propylene carbonate)

Zhihao Zhang [a,b,*], Qiang Shi [a,c], Juan Peng [a,c], Jianbin Song [a,c], Qingyong Chen [a,c], Junliang Yang [a,c], Yumei Gong [a,c], Ronghua Ji [a,c], Xiaofeng He [a], Joong-Hee Lee [b]

[a] *State Key Laboratory of Polymer Physics and Chemistry, Changchun Institute of Applied Chemistry, Chinese Academy of Sciences, 5625 People Street, Changchun 130022, PR China*

[b] *Polymer BIN Fusion Research Team, School of Advanced Materials Engineering, Chonbuk National University, Duckjin-dong 1Ga 664-14, Jeonju, Jeonbuk 561-756, Republic of Korea*

[c] *Graduate School of the Chinese Academy of Sciences, PR China*

Received 8 January 2006; received in revised form 10 September 2006; accepted 24 September 2006
Available online 17 November 2006

Abstract

Maleated poly(propylene carbonate) (PPC-MA)/organo-montmorillonite (OMMT) nanocomposites were first prepared via melt end-capping poly(propylene carbonate) (PPC) with maleic anhydride (MA) and melt-mixing the PPC-MA with commercial OMMT without and with hydroxyl groups in surfactants: Cloisite 20A (C20A) and Cloisite 30B (C30B), respectively. Intercalated and partially delaminated morphologies were corroborated via X-ray diffraction (XRD) and transmission electron microscopy (TEM). Dynamic mechanical analysis (DMA) revealed that PPC-MA was evidently reinforced by the partially delaminated C30B platelets. From XRD patterns of statically annealed PPC-MA/C20A and PPC-MA/C30B mixtures and Fourier transform infrared (FTIR) results of equivalent nanocomposites, partial delamination of C30B in PPC-MA was confirmed to be relevant to diffusion of PPC-MA molecular chains in C30B galleries, grafting of PPC-MA to C30B platelet surfaces and further separation of C30B platelets.

Keywords: Partial delamination; Organo-montmorillonite; Maleated poly(propylene carbonate)

1. Introduction

Poly(propylene carbonate) (PPC) is a copolymer of carbon dioxide with propylene oxide [1–3]. Fixation of carbon dioxide can mitigate the dreadful atmospheric pollution and utilize the abundant and low-cost natural resources. Owing to biodegradability and thermoplasticity, PPC has been processed into biomedical and packing materials. Nevertheless, the flexible carbonate groups in backbone chains have created many blemishes, including non-crystallizability, weaker processing stability and poorer mechanical properties.

The incorporation of a little organo-montmorillonite (OMMT) to polymers will result in the outstanding improvement of general properties [4–8]. Melt-mixing polymer with eco-friendly and low-cost OMMT has been an excellent technique [4–10] due to the pollution-free process and industrial feasibility. However, polymer nanocomposites with some other nanoparticles such as graphite nanosheet cannot be prepared by the similar method [11]. So the fabrication of PPC/OMMT nanocomposites via melt-compounding is a potential route to extend usages for biodegradable polymers and engineering plastics.

Unfortunately, PPC easily degrades when subjected to statically thermal treatment even at 180 °C [12]. In the dynamic shear field, heat derived from melt-processing makes material temperature 20–30 °C higher than barrel temperature and the degradation becomes more severe. Therefore, melt-mixing PPC with OMMT to prepare the nanocomposites will

* Corresponding author. State Key Laboratory of Polymer Physics and Chemistry, Changchun Institute of Applied Chemistry, Chinese Academy of Sciences, 5625 People Street, Changchun 130022, PR China. Tel.: +86 431 5262963; fax: +86 431 5262126.
E-mail address: zhangzh@ciac.jl.cn (Z. Zhang).

0032-3861/$ - see front matter © 2006 Elsevier Ltd. All rights reserved.
doi:10.1016/j.polymer.2006.09.041

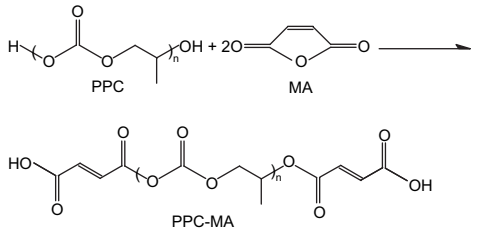

Scheme 1. Melt end-capping PPC with MA.

encounter more difficulties and challenges than fabrications of nanocomposites based on the other thermoplastic polymers [13–17].

Polymer/OMMT nanocomposites can be sorted into intercalated and exfoliated or delaminated structures. Owing to the homogeneous dispersion of individual silicate platelets in the polymer matrix, full exfoliated state is one of the ultimate aims in preparing polymer/OMMT nanocomposites [18]. However, only a few polymers, such as nylon 6 [19,20] and maleated polyethylene [18], have been melt-mixed with OMMT to achieve exfoliated structures, because it is very hard to separate the tightly stacked silicate platelets with van der Waals gap. Thus, melt-mixing PPC with OMMT to fabricate the exfoliated or delaminated, even partially delaminated nanocomposites with optimal properties is of academic significance and industrial merit.

In this contribution, intercalated and partially delaminated nanocomposites of maleated PPC (PPC-MA)/OMMT were prepared by melt end-capping PPC with maleic anhydride (MA) (Scheme 1) and melt-mixing the PPC-MA with OMMT. Commercial OMMT without and with hydroxyl groups in surfactants: Cloisite 20A (C20A) and Cloisite 30B (C30B), respectively, were selected. Morphologies were corroborated via X-ray diffraction (XRD) and transmission electron microscopy (TEM). Mechanical properties were investigated by dynamic mechanical analysis (DMA). Partial delamination mechanism of C30B in PPC-MA was clarified via XRD patterns of statically annealed PPC-MA/C20A and PPC-MA/C30B mixtures and Fourier transform infrared (FTIR) results of equivalent nanocomposites. To our best knowledge, there has not yet been paper on PPC-MA/OMMT nanocomposite.

2. Experimental

2.1. Materials

Totally biodegradable poly(propylene carbonate) (PPC) with a number average molecular weight of 7.2×10^4 and a polydispersity of 6.49, synthesized via the copolymerization of carbon dioxide and propylene oxide with a ternary rare earth metal catalyst [21,22], was supplied by Melic Sea High-Tech Group Company, Internal Mongolia. The carbonate unit content, estimated from ^{1}H NMR spectrum using the method described elsewhere [23,24], was 95.76%. Analytical grade maleic anhydride (MA) was obtained from Beijing Yili Fine Chemical Co., Ltd. Commercial organo-montmorillonites (OMMT) Cloisite 20A (C20A) and Cloisite 30B (C30B), montmorillonites exchanged by quaternary ammonium salts, with characteristics given in Table 1, were purchased from Southern Clay Products, Inc.

Table 1
Characteristics of OMMTs

OMMT	Cationic exchange capacity (mequiv/100 g)	Quaternary ammonium salt
C20A	95	$(CH_3)_2(HT)_2N^+Cl^-$
C30B	90	$CH_3T(CH_2CH_2OH)_2N^+Cl^-$

T = tallow; HT = hydrogenated tallow (C18, ~65%; C16, ~30%; C14, ~5%).

2.2. Preparation of nanocomposite

PPC was triturated, passed through a 20 mesh sieve and dried under vacuum at 55 °C for 2 days. Powdered MA and OMMT were dried under vacuum at room temperature and 80 °C, respectively, for 24 h. Nanocomposites were fabricated by mixing 93.1 parts of PPC and 1.9 parts of MA, melt-blending in a Haake Rheomix 600P internal mixer at a barrel temperature of 160 °C and a rotation speed of 60 rpm for 5 min and adding 5 parts of OMMT for another 5 min. PPC-MA was prepared at the same temperature, speed and time. For elucidating the crucial role in which PPC-MA played, PPC/OMMT nanocomposites were fabricated by mixing 95 parts of PPC and 5 parts of OMMT and melt-compounding at the same temperature and speed for 5 min.

2.3. Characterization

Number average molecular weight and molecular weight polydispersity were measured on a Waters 410 GPC system at 35 °C using tetrahydrofuran as the eluent and monodisperse polystyrene as the standard.

Grafting degree of PPC-MA (G) was defined as weight percent of grafted MA in PPC and determined from the titration of the purified PPC-MA, similar to that of the purified polypropylene-graft-maleic anhydride [25]. PPC-MA was dissolved in chloroform at a concentration of 5 w/v% and precipitated by ethanol. The dissolution/precipitation procedure was repeated twice again to completely remove ungrafted MA. The purified PPC-MA was dried under vacuum at 55 °C for 2 days. 1.0 g of the well-dried PPC-MA was dissolved in 100 ml chloroform. The solution was titrated with 0.01 N potassium hydroxide solution in methanol using phenolphthalein as the indicator. A blank test for PPC was carried out by the same method. G was calculated from Eq. (1):

$$G(\mathrm{wt}\%) = \frac{\frac{V_1 - V_0}{1000} \cdot N \cdot M_{\mathrm{MA}}}{2W} \times 100\% = \frac{(V_1 - V_0) N M_{\mathrm{MA}}}{2W 1000} \times 100\% \quad (1)$$

where, V_1 (ml) is base volume used for PPC-MA, V_0 (ml) the base volume used for neat PPC, N (mol/l) the base

concentration, W (g) the weight of sample and M_{MA} (g/ml) the molecular weight of MA with a value of 98.06.

Reaction degree between PPC and MA (R) was defined as weight percent of actual grafted MA in theoretical grafted MA deduced from Scheme 1:

$$R(\%) = \frac{GW_0}{2M_{MA}W_0/M_{n,0}} \times 100\% = \frac{GM_{n,0}}{2M_{MA}} \times 100\% \quad (2)$$

where, W_0 (g) is weight of neat PPC and $M_{n,0}$ (g/mol) the number average molecular weight of neat PPC.

XRD patterns were acquired using a Rigaku D/MAX 2500V X-ray diffractometer under $CuK_{\alpha 1}$ radiation (wavelength 0.15406 nm) operated at 40 kV and 200 mA. Data were collected continually between 0.5 and 10° at a speed of 2°/min and a step width of 0.02°.

TEM was operated with a Hitachi H800 at an accelerating voltage of 200 kV on ultrathin sections, less than 100 nm in thickness, of nanocomposites microtomed at −90 °C by LKB-5 ultramicrotome.

DMA was conducted with a NETZSCH DMA 242 in the single cantilever mode at a fixed frequency of 1 Hz and a rate of 2 °C/min heating from −50 to 100 °C. The maximum strain of 0.75% and the maximum dynamic force of 1 N were employed. Each sample was measured three times and medium value was taken.

FTIR spectra with a resolution of 2 cm^{-1} and an average of 64 scans were recorded on a Bruker IFS66v/S spectrometer. OMMT disks were fabricated by mixing powders with KBr and then compressing the mixtures. Nanocomposite and PPC-MA films were prepared by directly casting 1 wt% chloroform solutions on KBr pellets and evaporating the solvent slowly. Disk and film thickness was adjusted so that Beer–Lambert law is valid. Disturbances of solvent, moisture and carbon dioxide were removed completely by blowing nitrogen gas and vacuumizing. Measurements were performed under vacuum.

3. Results and discussion

3.1. Choice of preparation approach and conditions

Capping the terminal hydroxyl groups of PPC can restrain from chain unzipping degradation and enhance thermal stability [12]. Generally, PPC reacts with end-capping agents in solution. Melt end-capping PPC with biodegradable MA (Scheme 1) was chosen for the sake of industrialization and end usages as biodegradable materials.

Kuznetsov and Balazs [26] used the scaling theory to find that organically modified clay surfaces can be separated more readily in a melt of reactive difunctionalized chains than in a melt mixture of reactive difunctionalized chains and a nonreactive polymer. The carboxyl groups (COOH) on the two ends of PPC-MA chains are more active than the carbonate groups on the one end of PPC and can react more easily with hydroxyl groups (OH) of C30B. Therefore, C30B can peel off more easily in a melt of PPC-MA chains. Excessive MA was used to entirely convert PPC into PPC-MA just before melt-mixing with OMMT. G obtained from Eq. (1) was 0.26% and R calculated from Eq. (2) 95.45%. Larger R but smaller G mean that most PPC reacted with a small amount of MA, due to higher M_n and fewer chain end groups of PPC, to produce PPC-MA together with ungrafted MA.

On the other hand, medium shear favors the diffusion of PPC-MA in OMMT galleries. Higher barrel temperature encourages the reactions and makes PPC-MA tethered to C30B platelet surfaces. Both of them profit the separation of C30B platelets. Undergoing such violent dynamic shearing, however, neat PPC degraded to some degree, as inferred from the declining torque until 1.71 Nm. Variations of torque vs compounding time for PPC/C20A and PPC/C30B nanocomposites were similar to that for neat PPC and end torques for PPC/C20A and PPC/C30B nanocomposites were 1.43 and 1.14 Nm, respectively (Fig. 1a). C20A and C30B decreased the end torque of PPC, perhaps they made the degradation of PPC somewhat worse and decreased molecular weight and viscosity because the torque is an embodiment of viscosity

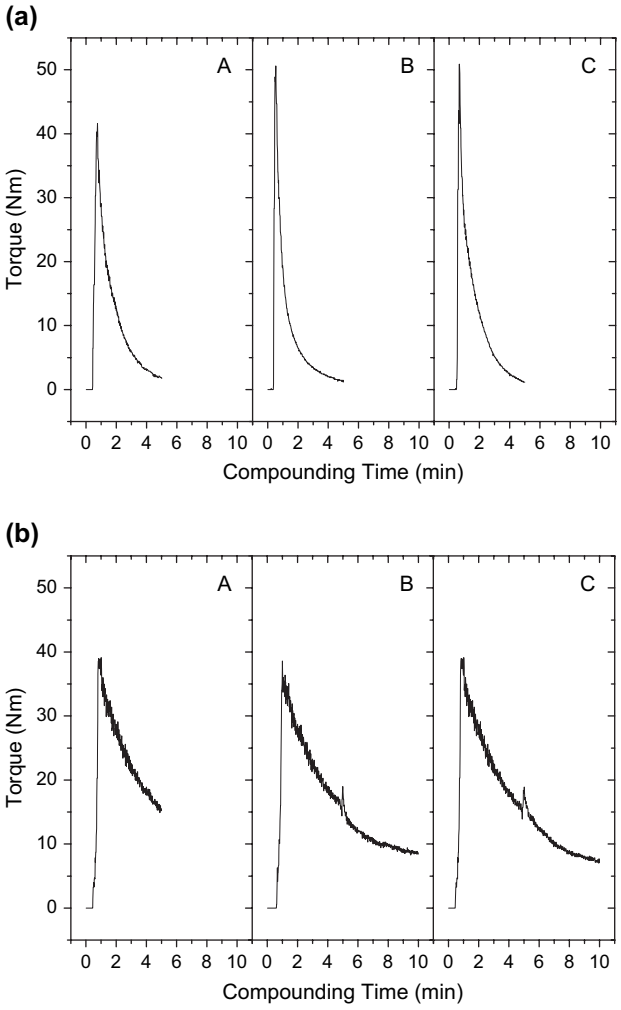

Fig. 1. Torque vs compounding time of (a): (A) neat PPC, (B) PPC/C20A nanocomposite and (C) PPC/C30B nanocomposite and (b): (A) PPC-MA, (B) PPC-MA/C20A nanocomposite and (C) PPC-MA/C30B nanocomposite.

[27]. These behaviors are opposed to those observed by Kader and Nah that the presence of organoclay increased the torque value [28]. The melt-processed PPC, PPC/C20A and PPC/C30B nanocomposites became viscous and soft, apparently owning no applicable value. Wonderfully, end torques of PPC-MA, PPC-MA/C20A and PPC-MA/C30B nanocomposites were 15.20, 8.43 and 7.71 Nm (Fig. 1b) and much larger than those for PPC, PPC/C20A and PPC/C30B nanocomposites, respectively. These phenomena reveal MA remarkably enhanced the thermal and thus the processing stabilities of PPC and exhibited the viscosity enhancement effect by the delaminated clay very well. Therefore, end-capping PPC is vital to successfully preparing PPC nanocomposite via melt-compounding.

3.2. Morphology

Fig. 2 presents XRD patterns of OMMTs, PPC-MA and PPC-MA/OMMT nanocomposites. In Fig. 2a, pure C20A had the *d*-spacing of (001) plane of 2.42 nm. Non-crystalline PPC-MA showed no diffraction peak between 0.5 and 10°, indicating that diffraction peaks of the nanocomposite arose from C20A alone. For PPC-MA/C20A nanocomposite, the *d*-spacing of (001) plane increased 58.68% to 3.84 nm with the shift of the diffraction peak to a lower angle. The smaller peak with the *d*-spacing of 1.92 nm corresponded to (002) plane. All these observations reveal that PPC-MA was intercalated into C20A galleries.

The spacing of (001) plane for pure C30B was 1.81 nm (Fig. 2b). In contrast with PPC-MA/C20A nanocomposite, no diffraction peak for PPC-MA/C30B nanocomposite appeared. Morgan and Gilman suggested that the absence of diffraction peak probably results from delaminated nanocomposite, disordered intercalated nanocomposite and so on [29]. Therefore, TEM was used to distinguish one morphology from the others.

Fig. 3 exhibits TEM micrographs of nanocomposites. Intercalated C20A tactoids were stacked and flocculated in PPC-MA (Fig. 3a), whereas C30B was delaminated into 5–10 layer multiplatelet aggregates in polymer matrix (Fig. 3b). Therefore, PPC-MA/C30B nanocomposite bore partially delaminated structure.

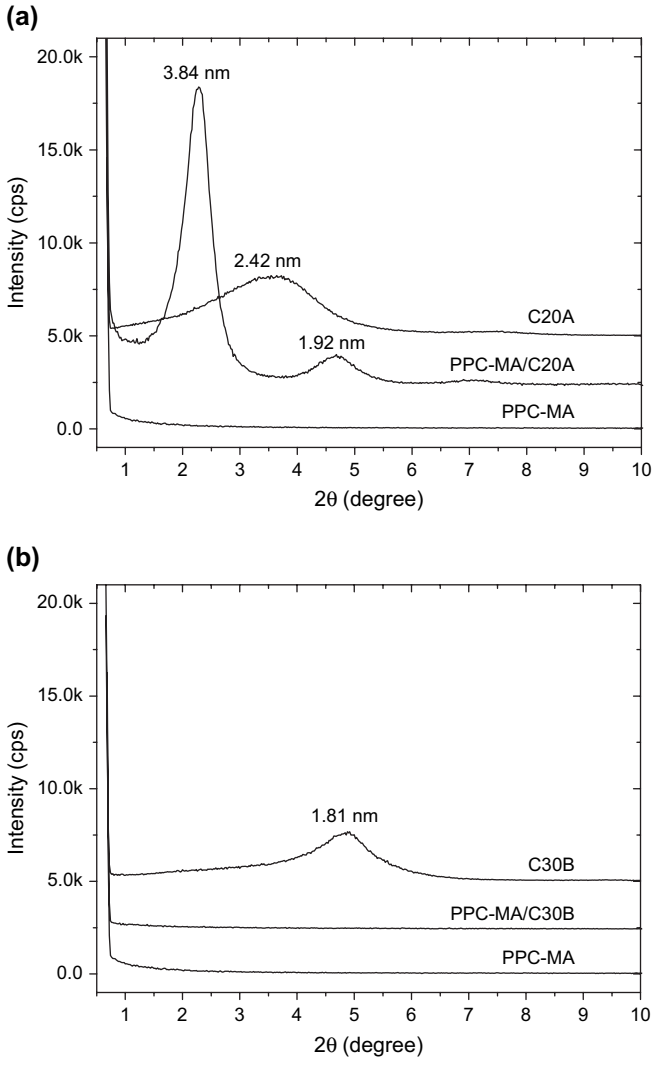

Fig. 2. XRD patterns of (a) C20A, PPC-MA and PPC-MA/C20A nanocomposite and (b) C30B, PPC-MA and PPC-MA/C30B nanocomposite.

3.3. Mechanical properties

Dependence of storage modulus (E') and loss tangent ($\tan\delta$) for PPC-MA and nanocomposites on temperature is demonstrated in Fig. 4. Within the lower temperature range, all samples were in the glassy region and E' values decreased very slowly with the temperature up to ca. 25 °C (Fig. 4a). The glassy modulus of PPC-MA was reinforced with the addition of the OMMT. At the initial temperature −50 °C, C20A merely increased E' of PPC-MA 41.29%. Contrastively, C30B strengthened 91.88% (Table 2). Raising the temperature continually to ca. 40 °C, E' values of all samples underwent rapid drops, resulting from the energy dissipation during glass–rubber relaxation [30]. At still higher temperatures, E' values of all samples tended to constants, indicating the formations of rubber-like structures. C30B also enhanced the rubbery modulus of PPC-MA. With the temperature increasing to 50 °C, E' of PPC-MA was improved 33.67% by C20A and 61.44% by C30B, respectively, also seen from Table 2, suggesting that the nanocomposite stiffness in the rubbery region was also dominated by C30B. These behaviors are due to the restricted movement of polymer chains [16]. Clearly, the OMMT reinforced PPC-MA in the whole temperature range. The enhancements in the glassy modulus were greater than those in the rubbery modulus, indicating that these nanocomposites can be potentially used as cryogenic materials. Moreover, $\tan\delta$ values of all samples showed maxima in glass–rubber transition region (Fig. 4b), arising from the release of cooperative motions of long amorphous chains at glass transition temperature (T_g) and the compatibility between PPC-MA and the OMMTs. T_g of PPC-MA shifted to higher temperatures, 6.50 and 7.20 °C, upon the C20A and C30B addition, respectively, because the nanometer size maximizes the adhesion between the polymer and the layered

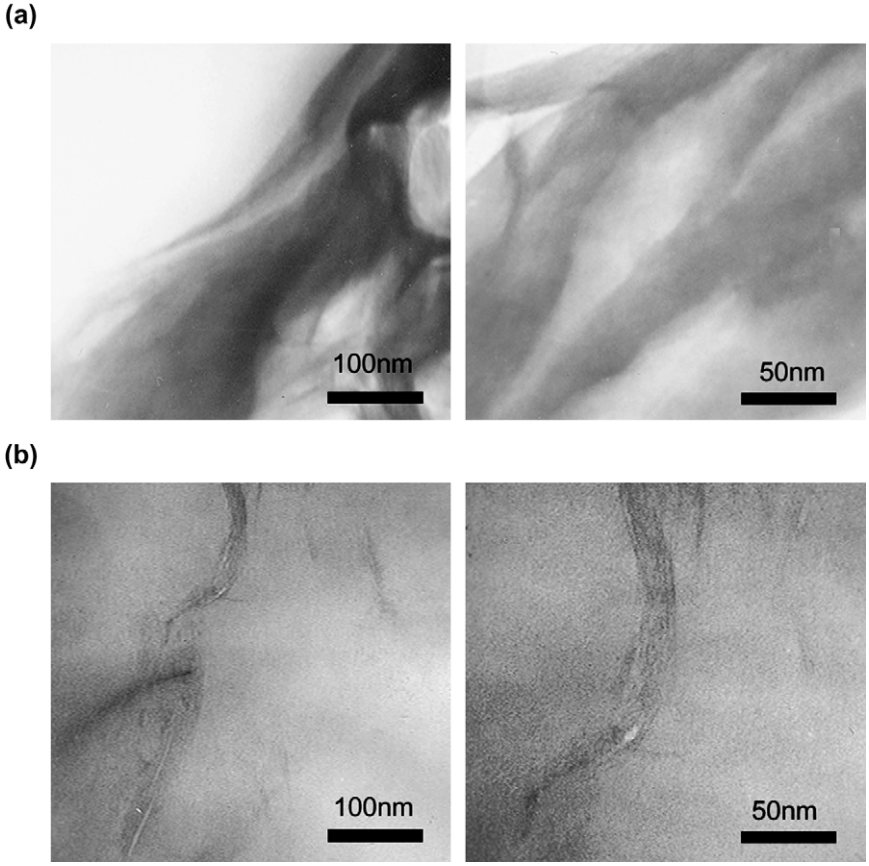

Fig. 3. TEM bright field images of (a) PPC-MA/C20A nanocomposite and (b) PPC-MA/C30B nanocomposite.

silicate surfaces so as to restrict segmental motion near the organic–inorganic interface [31].

Of the two nanocomposites, PPC-MA/C30B achieved a greater E' and a higher T_g because of a higher degree of dispersion and a stronger covalent linkage between PPC-MA and C30B.

3.4. Partial delamination mechanism of C30B in PPC-MA

Ginzburg et al. [32] reported the exfoliated structure of polymer melt/organic modified clay mixture is dependent on length and/or density of polymer chains grafted on organoclay. Danumah et al. [33] put forward three steps to obtain partial or full exfoliation of the nanoparticles inside the polymeric matrix: (1) Diffusion of the macromolecular chains inside the relatively open interlamellar galleries, typical spacing of 3–6 nm, under flow or quiescent conditions. (2) Interactions between the nanoparticle surfaces and the diffusing macromolecular chains, including entanglements, covalent bonding, hydrogen bonding or electrostatic bonding. (3) Delamination of the nanoparticle layers due to external strong stresses, such as shear stress. Partial delamination mechanism of C30B in PPC-MA was tried to clarify with experiment evidence.

Hu and Zhao investigated the effects of annealing on polymorphic structure of nylon 6/silicate nanocomposite [34]. To determine the effect of quiescent conditions on partial delamination of C30B in PPC-MA, PPC-MA/C20A and PPC-MA/C30B mixture were statically annealed at the same temperature for the same time as equivalent nanocomposites during melt-compounding. As shown in Fig. 5, all annealed samples obtained the intercalated structures due to Brownian motion. The *d*-spacing of (001) plane for PPC-MA/C20A nanocomposite was larger than that for annealed PPC-MA/C20A mixture. Comparatively, PPC-MA/C30B nanocomposite owned the partially delaminated structure but annealed PPC-MA/C30B mixture exhibited the intercalated structure. It is concluded from all these observations that statically annealing PPC-MA/OMMT mixtures for 5 min encouraged the intercalation whereas shear stress diffused the macromolecular chains in OMMT galleries and further either expanded the galleries of C20A or peeled apart the C30B platelets.

To understand the reactions between C30B and PPC-MA, FTIR was employed. C20A showed stretching absorptions of hydroxyl groups of silanol ($OH_{silanol}$) and absorbed water ($H_2O_{absorbed}$) at 3632.6 and 3427.2 cm^{-1}, respectively, and a weak bending absorption of $H_2O_{absorbed}$ at 1639.4 cm^{-1} (Fig. 6). Counterparts of C30B were at 3633.6, 3411.8 and 1639.4 cm^{-1}, respectively. Stretching absorption at 3411.8 cm^{-1} was also ascribed to hydroxyl groups of surfactant ($OH_{surfactant}$) in C30B [35,36].

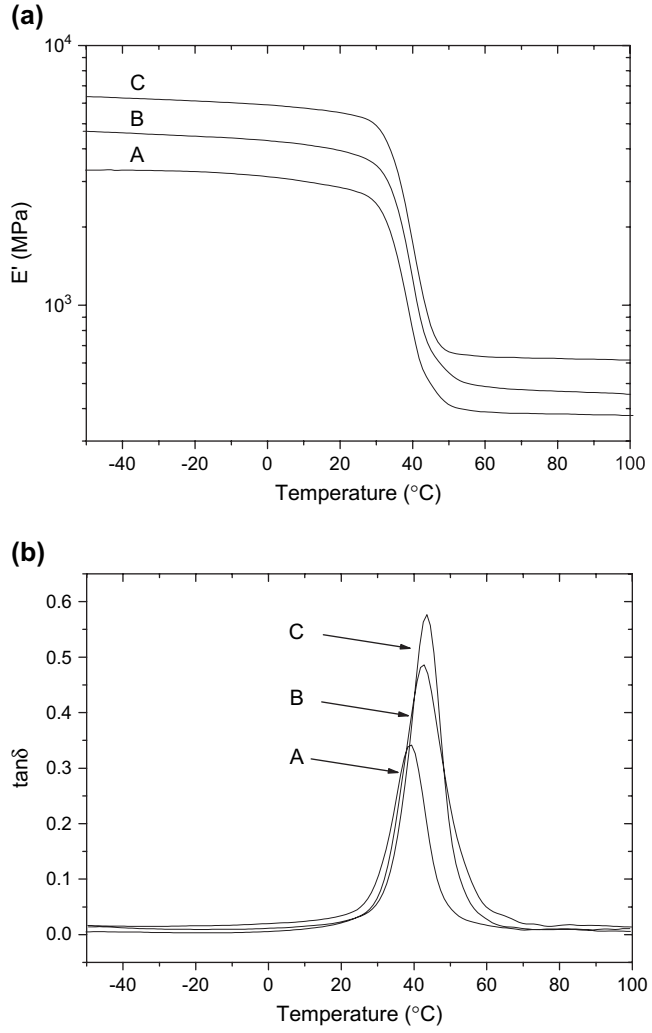

Fig. 4. Dependence of (a) storage modulus E' and (b) loss tangent $\tan\delta$ for (A) PPC-MA (B) PPC-MA/C20A nanocomposite and (C) PPC-MA/C30B nanocomposite on temperature.

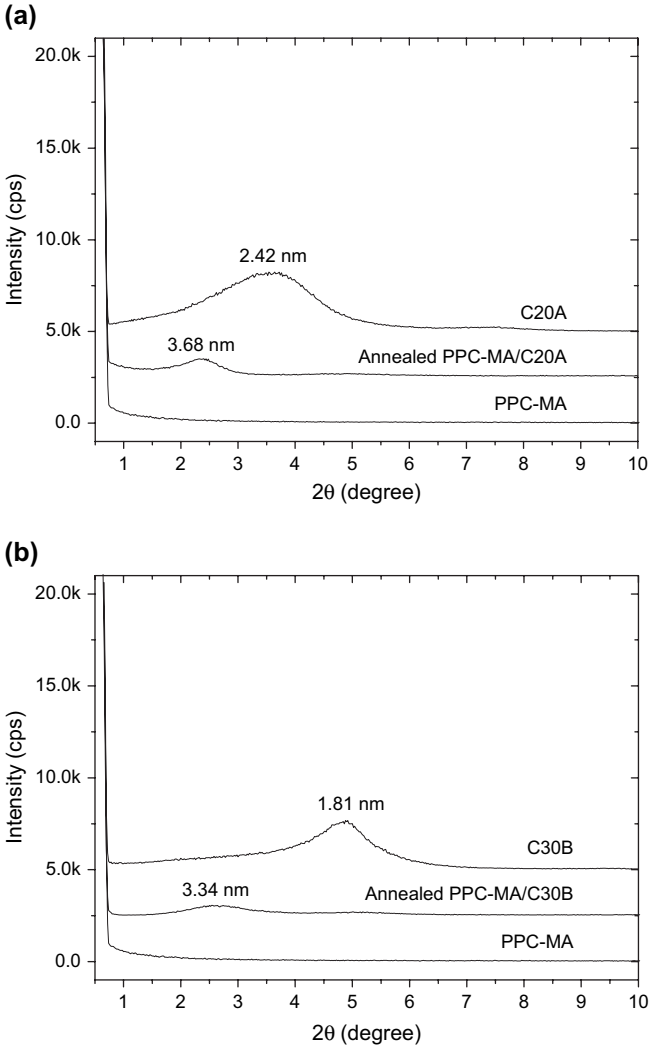

Fig. 5. XRD patterns of (a) C20A, PPC-MA and annealed PPC-MA/C20A mixture and (b) C30B, PPC-MA and annealed PPC-MA/C30B mixture.

In Fig. 7, stretching absorptions of carbonyl groups (C═O) of PPC-MA and nanocomposites were situated at 1747.4 cm^{-1}. Width of stretching absorption of C═O of PPC-MA/C30B nanocomposite was narrower than that of PPC-MA, because stretching absorptions of free and hydrogen-bonded carbonyl groups ($C{=}O_{free}$ and $C{=}O_{H\text{-}bonded}$) of carboxyl groups (COOH) are higher and lower than 1750 cm^{-1}, respectively. When COOH of PPC-MA reacted with OH of OMMT to create ester bonds (COOC), $C{=}O_{free}$ and $C{=}O_{H\text{-}bonded}$ diminished. These phenomena imply that more $COOH_{free}$ and $COOH_{H\text{-}bonded}$ in PPC-MA were exhausted by both $OH_{silanol}$ and $OH_{surfactant}$ in C30B than by only $OH_{silanol}$ in C20A (Scheme 2) and more PPC-MA was tethered to the C30B platelet surfaces. Therefore, C30B had a higher level of delamination and a better degree of dispersion in PPC-MA than C20A.

Table 2
Dynamic mechanical properties and increments for PPC-MA, PPC-MA/C20A nanocomposite and PPC-MA/C30B nanocomposite

	T (°C)	PPC-MA	PPC-MA/C20A		PPC-MA/C30B	
E' (MPa)	−50	3311.09	4678.29	41.29%	6353.29	91.88%
	0	3119.60	4305.50	38.14%	5912.63	89.53%
	50	410.10	548.19	33.67%	662.07	61.44%
	100	376.48	454.85	20.82%	615.98	63.62%
T_g (°C)		36.31	42.81	6.50	43.51	7.20

Macromolecular chains are so long and flexible that they entangle one another. There also existed entanglements among free and tethered PPC-MA chains. It is via these entanglements that shear stress was transferred to OMMT platelets.

All the factors combined together to promote the partial delamination of C30B in PPC-MA. These results confirm the hypotheses proposed by Danumah et al. [33].

4. Conclusions

Intercalated PPC-MA/C20A and partially delaminated PPC-MA/C30B nanocomposites were successfully prepared via melt end-capping and melt-compounding technologies.

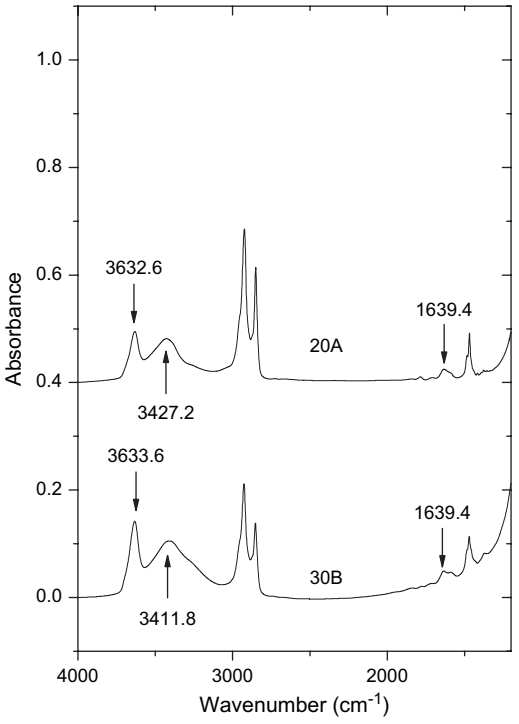

Fig. 6. FTIR spectra of C20A and C30B at room temperature.

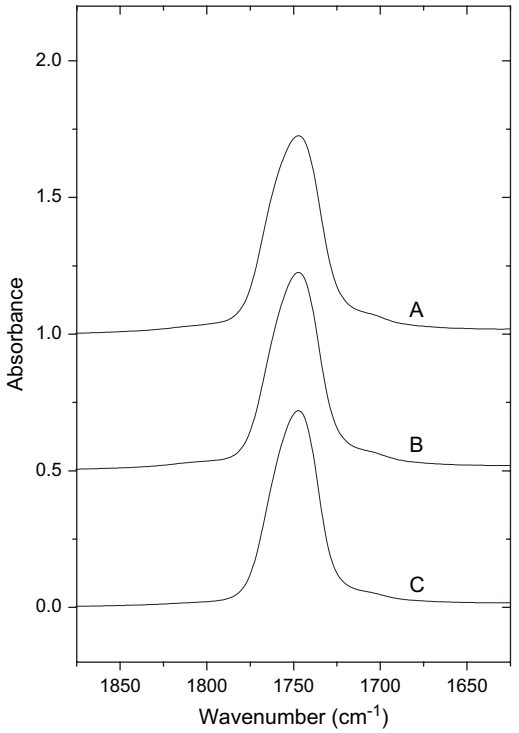

Fig. 7. FTIR spectra at room temperature in the carbonyl stretching range: (A) PPC-MA (B) PPC-MA/C20A nanocomposite and (C) PPC-MA/C30B nanocomposite.

Intercalated C20A tactoids were flocculated in PPC-MA, whereas C30B was partially delaminated into 5–10 layer multiplatelet aggregates in the polymer matrix. Mechanical properties of PPC-MA were markedly reinforced by the partially delaminated C30B platelets. Partial delamination mechanism of C30B in PPC-MA was clarified via experimental evidence: statically annealing PPC-MA/C30B mixture for 5 min merely intercalated PPC-MA chains into the C30B galleries due to Brownian motion. Shear stress also diffused PPC-MA in OMMT galleries. Reactions between PPC-MA and C30B tethered PPC-MA to the C30B platelet surfaces. Shear stress further peeled apart the C30B platelets in PPC-MA.

The entanglements among free and tethered PPC-MA chains transferred the shear stress to the C30B platelets. We are trying to verify the entanglements via rheology. The enhancements of C30B on PPC-MA in the other properties, such as gas barrier properties, flammability and biodegradability and the fabrications of a higher delamination level of PPC

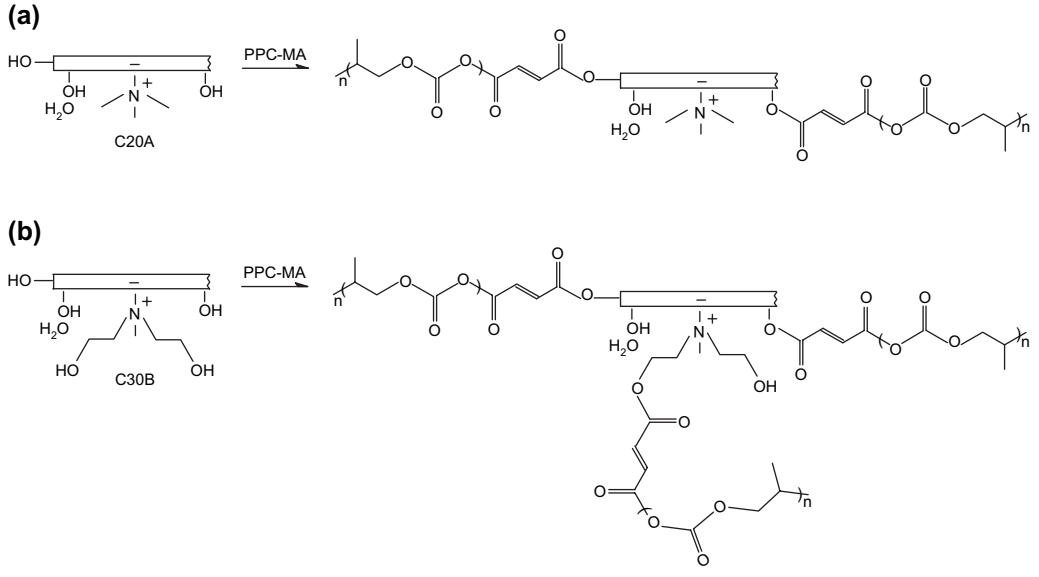

Scheme 2. Proposed reactions between OMMT and PPC-MA.

nanocomposites based on other clays or organoclays under milder conditions are also being investigated.

Acknowledgments

The work was financially supported by the Ministry of Science and Technology of China (Project No. 2003AA302530) and the National Natural Science Foundations of China (Project No. 50473029 and 20374051). The authors are indebted to the grant of Post-doc Program, Chonbuk National University and 2nd Phase BK21 program granted by Ministry of Education and Human Resources Development of Korea.

References

[1] Inoue S, Koinuma H, Tsuruta T. J Polym Sci Polym Lett Ed 1969;7: 287–92.
[2] Darensbourg DJ, Holtcamp MW. Macromolecules 1995;28:7577–9.
[3] Mang S, Cooper AI, Colclough ME, Chauhan N, Holmes AB. Macromolecules 2000;33:303–8.
[4] Kojima Y, Usuki A, Kawasumi M, Okada A, Kurauchi T, Kamigaito O. J Appl Polym Sci 1993;49:1259–64.
[5] Kawasumi M, Hasegawa N, Kato M, Usuki A, Okada A. Macromolecules 1997;30:6333–8.
[6] Wang Z, Pinnavaia TJ. Chem Mater 1998;10:3769–77.
[7] Alexandre M, Dubois P. Mater Sci Eng 2000;R28:1–63.
[8] Yeh J-M, Liou S-J, Lin C-Y, Cheng C-Y, Chang Y-W, Lee K-R. Chem Mater 2002;14:154–61.
[9] Vaia RA, Ishii H, Giannelis EP. Chem Mater 1993;5:1694–6.
[10] Giannelis EP, Krishnamoorti R, Manias E. Adv Polym Sci 1999;138: 107–47.
[11] Mo Z, Sun Y, Chen H, Zhang P, Zuo D, Liu Y, et al. Polymer 2005;46: 12670–6.
[12] Dixon DD, Ford ME, Montell GJ. J Polym Sci Polym Lett Ed 1980;18: 131–4.
[13] Viville P, Lazzaroni R, Pollet E, Alexandre M, Dubois P, Borcia G, et al. Langmuir 2003;19:9425–33.
[14] Gilman JW, Jackson CL, Morgan AB, Harris Jr R, Manias E, Giannelis EP, et al. Chem Mater 2000;12:1866–73.
[15] Lee KM, Han CD. Polymer 2003;44:4573–88.
[16] Sinha Ray S, Maiti P, Okmoto M, Yamada K, Ueda K. Macromolecules 2002;35:3104–10.
[17] Fornes TD, Hunter DL, Paul DR. Macromolecules 2004;37:1793–8.
[18] Koo CM, Ham HT, Kim SO, Wang KH, Chung IJ, Kim D-C, et al. Macromolecules 2002;35:5116–22.
[19] Liu L, Qi Z, Zhu X. J Appl Polym Sci 1999;71:1133–8.
[20] Fornes TD, Yoon PJ, Keskkula H, Paul DR. Polymer 2001;42:9929–40.
[21] Zhao X, Wang X, Wang F. US patent 0 082 363 A1; 2002.
[22] Zhao X, Wang X, Wang F, Min J, Zhou Q. Japanese patent 386 806; 2003.
[23] Chen X, Shen Z, Zhang Y. Macromolecules 1991;24:5305–8.
[24] Zhang Z, Mo Z, Zhang H, Wang X, Zhao X. Macromol Chem Phys 2003; 204:1557–66.
[25] Shi D, Yang J, Yao Z, Wang Y, Huang H, Jing W, et al. Polymer 2001;42: 5549–57.
[26] Kuznetsov DV, Balazs AC. J Chem Phys 2000;112:4365–75.
[27] Yudin VE, Divoux GM, Otaigbe JU, Svetlichnyi VM. Polymer 2005;46: 10866–72.
[28] Kader MA, Nah C. Polymer 2004;45:2237–47.
[29] Gilman JW, Morgan AB. J Appl Polym Sci 2003;87:1329–38.
[30] Azizi Samir MAS, Alloin F, Sanchez JY, El Kissi N, Dufresne A. Macromolecules 2004;37:1386–93.
[31] Agag T, Koga T, Takeichi T. Polymer 2001;42:3399–408.
[32] Ginzburg VV, Singh C, Balazs AC. Macromolecules 2000;33:1089–99.
[33] Danumah C, Bousmina M, Kaliaguine S. Macromolecules 2003;36: 8208–9.
[34] Hu X, Zhao X. Polymer 2004;45:3819–25.
[35] do Nascimento GM, Constantino VRL, Temperini MLA. J Phys Chem B 2004;108:5564–71.
[36] Madejova J, Komadel P. Clays Clay Miner 2001;49:410–32.